catalysts

MDPI

Article

# Synthesis of Mesoporous Cu-Ni/$Al_2O_4$ Catalyst for Hydrogen Production via Hydrothermal Reconstruction Route

**Kai-Jhei Lin [1], Yi-Kai Chih [2], Wei-Hsin Chen [2,3,4], Hsin-Kai Huang [1], Hong-Ping Lin [1,*] and Chun-Han Hsu [5,*]**

1 Department of Chemistry, National Cheng Kung University, Tainan 701, Taiwan; kaijhei@gmail.com (K.-J.L.); kite1029@yahoo.com.tw (H.-K.H.)
2 Department of Aeronautics and Astronautics, National Cheng Kung University, Tainan 701, Taiwan; chihyikai@gmail.com (Y.-K.C.); weihsinchen@gmail.com (W.-H.C.)
3 Research Center for Smart Sustainable Circular Economy, Tunghai University, Taichung 407, Taiwan
4 Department of Mechanical Engineering, National Chin-Yi University of Technology, Taichung 411, Taiwan
5 General Education Center, National Tainan Junior College of Nursing, Tainan 700, Taiwan
* Correspondence: hplin@mail.ncku.edu.tw (H.-P.L.); chhsu@ntin.edu.tw (C.-H.H.); Tel.: +886-2757575-65342 (H.-P.L.)

**Abstract:** Mesoporous Cu-Ni/$Al_2O_4$ catalyst of high surface area (176 $m^2g^{-1}$) is synthesized through a simple hydrothermal reconstruction process by using low-cost activated alumina as the aluminate source without organic templates. The desired mesoporous structure of the catalyst is formed by the addition of $Cu^{2+}$ and $Ni^{2+}$ metal ions in the gel solution of the activated alumina followed by hydrothermal treatment at 70 °C and calcination at temperatures in the range of 600 to 800 °C. To consider the environmental concern, we found the concentration of the $Cu^{2+}$ and $Ni^{2+}$ ion in the residual filtrate is less than 0.1 ppm which satisfies the effluent standard in Taiwan (<1.0 ppm). The effects of the pH value, hydrothermal treatment time, and calcination temperature on the structure, morphology and surface area of the synthesized Cu-Ni/$Al_2O_4$ composites are investigated as well. In addition, the Cu-Ni/$Al_2O_4$ catalyst synthesized at pH 9.0 with a hydrothermal treatment time of 24 h and a calcination temperature of 600 °C is used for hydrogen production via the partial oxidation of methanol. The conversion efficiency is found to be >99% at a reaction temperature of around 315 °C, while the $H_2$ yield is 1.99 mol $H_2$/mol MeOH. The catalyst retains its original structure and surface area following the reaction process, and is thus inferred to have a good stability. Overall, the hydrothermal reconstruction route described herein is facile and easily extendable to the preparation of other mesoporous metal-alumina materials for catalyst applications.

**Keywords:** hydrothermal treatment; partial oxidation of methanol; hydrogen production

check for updates

**Citation:** Lin, K.-J.; Chih, Y.-K.; Chen, W.-H.; Huang, H.-K.; Lin, H.-P.; Hsu, C.-H. Synthesis of Mesoporous Cu-Ni/$Al_2O_4$ Catalyst for Hydrogen Production via Hydrothermal Reconstruction Route. *Catalysts* **2022**, *12*, 32. https://doi.org/10.3390/catal12010032

Academic Editor: José Antonio Calles

Received: 6 December 2021
Accepted: 27 December 2021
Published: 28 December 2021



## 1. Introduction

Current hydrogen production methods include mainly dry reforming [1], methane pyrolysis [2], steam reforming [3,4], partial oxidation [5,6], and autothermal steam reforming [7]. Among them, steam reforming has the advantage of a high hydrogen production yield. However, since it involves an endothermic reaction, it requires the continuous supply of heat energy to initiate the reaction process and then enable it to proceed. Consequently, partial oxidation is generally preferred since it is an exothermic process, and hence does not require the supply of additional heat [8,9].

Many noble catalysts, such as palladium [10] and platinum [11], have been used for the hydrogenation reaction of oxygen-containing molecules. However, such metals are expensive, and hence the problem of developing alternative lower-cost metals as catalysts for hydro-deoxygenation reactions has attracted great attention in the literature [12–14]. Auprêtre et al. [15] found that nickel catalysts provide many advantages for steam recombination reactions, including a high activity and a low cost. However, the nickel catalyst have

only a short useable life due to rapid inactivation by the transformation of coke (i.e., carbon deposition) on the active sites. Tu et al. [16] found that $Cu/SiO_2$ catalysts have an improved resistance to carbon deposition, and hence provide a longer life. Mariño et al. [17] used an impregnation method to support Cu-Ni precursors on alumina and used the resulting material as a catalyst in the production of hydrogen via the steam reforming of ethanol. The experimental results showed that a conversion rate of around 55% was obtained at a low reaction temperature of 300 °C. Hu et al. [18] synthesized nanoscale copper-cobalt catalysts on $Al_2O_3$ supports for the hydrogenation of acetylene. The results showed that the bimetallic catalyst improved the conversion compared to that achieved using pure Cu or Co catalysts through a synergistic effect. Several other recent studies have similarly shown that Cu-Ni bimetallic catalysts are more effective than single metal catalysts in low temperature steam reforming processes [19,20]. The aforementioned studies show that the bimetallic Cu-Ni catalysts with a synergistic effect improve the hydrogen conversion rate compared to that achieved using pure Cu or Ni catalysts through a synergistic effect. Here, the Ni-Cu catalysts can effectively promote the electronic effect between Ni and Cu, and enhance the adsorption and activation abilities of the corresponding catalyst for the reactant [21–23].

Commercial catalysts used for the production of hydrogen through the partial oxidation of methanol (POM) route have a high conversion rate of around 93~98%. However, they require a high reaction temperature of 500 °C, or more [24,25], and are thus expensive for large-scale production. Thus, in the present study, the low-cost activated alumina are used as the aluminate source, and the salts of the Cu, Ni metal precursors and aluminum hydroxide are then restructured through a simple low-temperature hydrothermal treatment process performed at 70 °C, Finally, the desired highly-dispersed porous Cu-Ni/$Al_2O_4$ composites with high-dispersity of the active sites are obtained from a high-temperature calcination process. Since our proposed synthesis method does not produce wastewater, which the concentration of the $Ni^{2+}$ and $Cu^{2+}$ ion in the residual filtrate is less than 0.1 ppm which satisfies the effluent standard in Taiwan (<1.0 ppm), it can be used as a basis for scaling up the production of catalysts. In addition, the proposed method not only avoid the concern on the residual $Cu^{2+}$ and $Ni^{2+}$ ion contents in the filtrate, but also achieves a hydrogen conversion efficiency of >99% at a low reaction temperature of 315 °C, and therefore significantly reduces the cost of large-scale hydrogen production.

## 2. Results and Discussion

### *2.1. Effect of pH on Kinetics of Cu-Ni/$Al_2O_4$ Formation*

For heterogeneous nucleation and growth of metal hydroxides on the porous matrixes, the pH value is a key factor in determining the precipitation rate and extent via interaction match of $Cu^{2+}$ and $Ni^{2+}$ precursors with aluminum hydroxide [26,27]. Accordingly, to determine the optimal pH value for the synthesis of the present Cu-Ni/$Al_2O_4$ composites, the preparation process was performed using a Ni:Cu:Al molar ratio = 1:10:100 at pH values of 6.0 to 10.0. Table 1 shows the residual quantities of $Cu^{2+}$ and $Ni^{2+}$ in the filtrate following the hydrothermal process under each of the pH conditions. For pH 6.0, pH 7.0 and pH 10.0, the concentrations of $Cu^{2+}$ and $Ni^{2+}$ exceed 1.0 ppm. Hence, it is inferred that the pH conditions fail to bring about the complete precipitation and dispersion of $Cu^{2+}$ and $Ni^{2+}$ during the synthesis process. However, at pH 8.0 and pH 9.0, the concentrations of $Cu^{2+}$ and $Ni^{2+}$ ions are so low that they cannot be detected. In other words, both metal ion precursors combine fully with the aluminum hydroxide. Notably, the N.D. condition of the $Cu^{2+}$ and $Ni^{2+}$ ions implies that both ions have concentrations of less than 0.1 ppm, and therefore satisfy the effluent standard in Taiwan (<1.0 ppm) [28,29]. Thus, the residual filtrate can be disposed of directly without the need for expensive and time-consuming waste treatment processing.

**Table 1.** Residual concentrations of copper and nickel ions in filtrate at different pH values.

| pH | [$Cu^{2+}$] in Filtrate/ppm | [$Ni^{2+}$] in Filtrate/ppm |
|---|---|---|
| 6.0 | 11.24 | 15.10 |
| 7.0 | N.D.* | 1.83 |
| 8.0 | N.D. | N.D. |
| 9.0 | N.D. | N.D. |
| 10.0 | 4.46 | N.D. |

* N.D. = Not Detected.

To investigate the structure of the as-prepared samples, all of the samples were calcined at 600 °C and then analyzed by XRD. As shown in Figure 1A, the XRD patterns of the products prepared at pH 6.0 and pH 10 contain sharp diffraction peaks at 2θ = 35 ° and 38 ° corresponding to CuO. By contrast, the samples prepared at pH 7.0–9.0 show broad peaks at 2θ = 37 ° and 67 ° corresponding to Cu-Ni/$Al_2O_4$. In other words, within the pH range of 7.0–9.0, the $Cu^{2+}$ and $Ni^{2+}$ ions can incorporate into the alumina structure with high dispersibility and no self-aggregation of CuO and NiO precipitates occurs. Figure 1B shows the nitrogen adsorption-desorption isotherms of the product synthesized at pH 9.0. The isotherms indicate that the Cu-Ni/$Al_2O_4$ composite has a type IV characteristic with H4 hysteresis loops (a sheet structure) and a BET surface area of 176 $m^2g^{-1}$. The TEM image presented in Figure 2A shows that the Cu-Ni/$Al_2O_4$ material prepared at pH 6.0 has a strong particulate aggregation morphology. However, for pH values in the range of pH 7 to pH 9 (Figure 2B–D), the products have a fine flake structure with mesopores. When the pH value is further increased to 10.0, the material structure changes from a flake structure to a rod-like structure with aggregation (Figure 2E). Based on these results above, a reaction condition of pH 9.0 was used in all the following experiments designed to determine the optimal synthesis conditions.

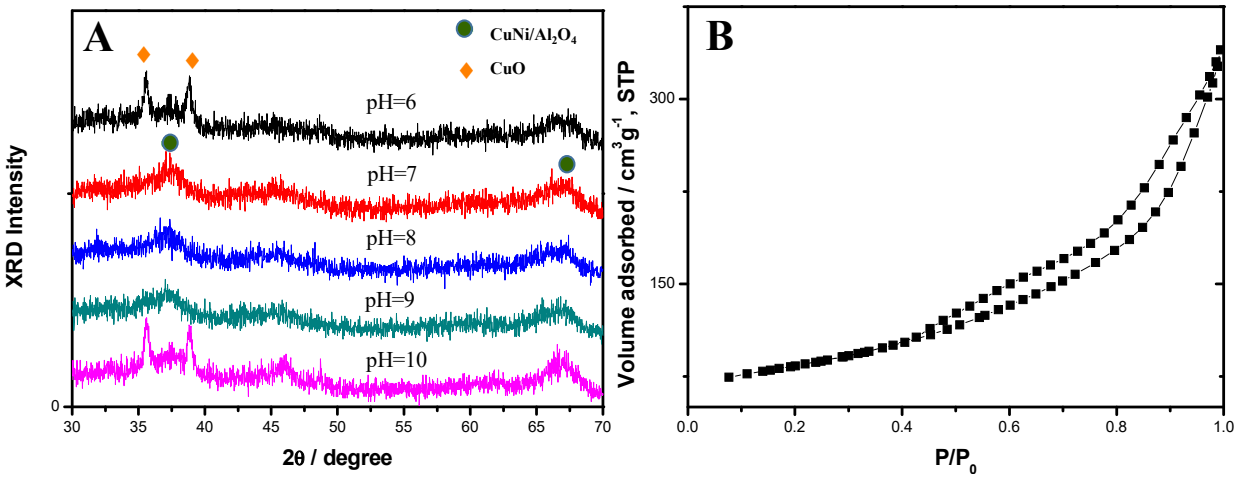


**Figure 1.** (**A**) XRD patterns of the Cu-Ni/$Al_2O_4$ samples synthesized under different pH conditions, and (**B**) nitrogen adsorption-desorption isotherms of the Cu-Ni/$Al_2O_4$ samples synthesized under pH 9.0. (Note that calcination temperature is 600 °C for all samples).

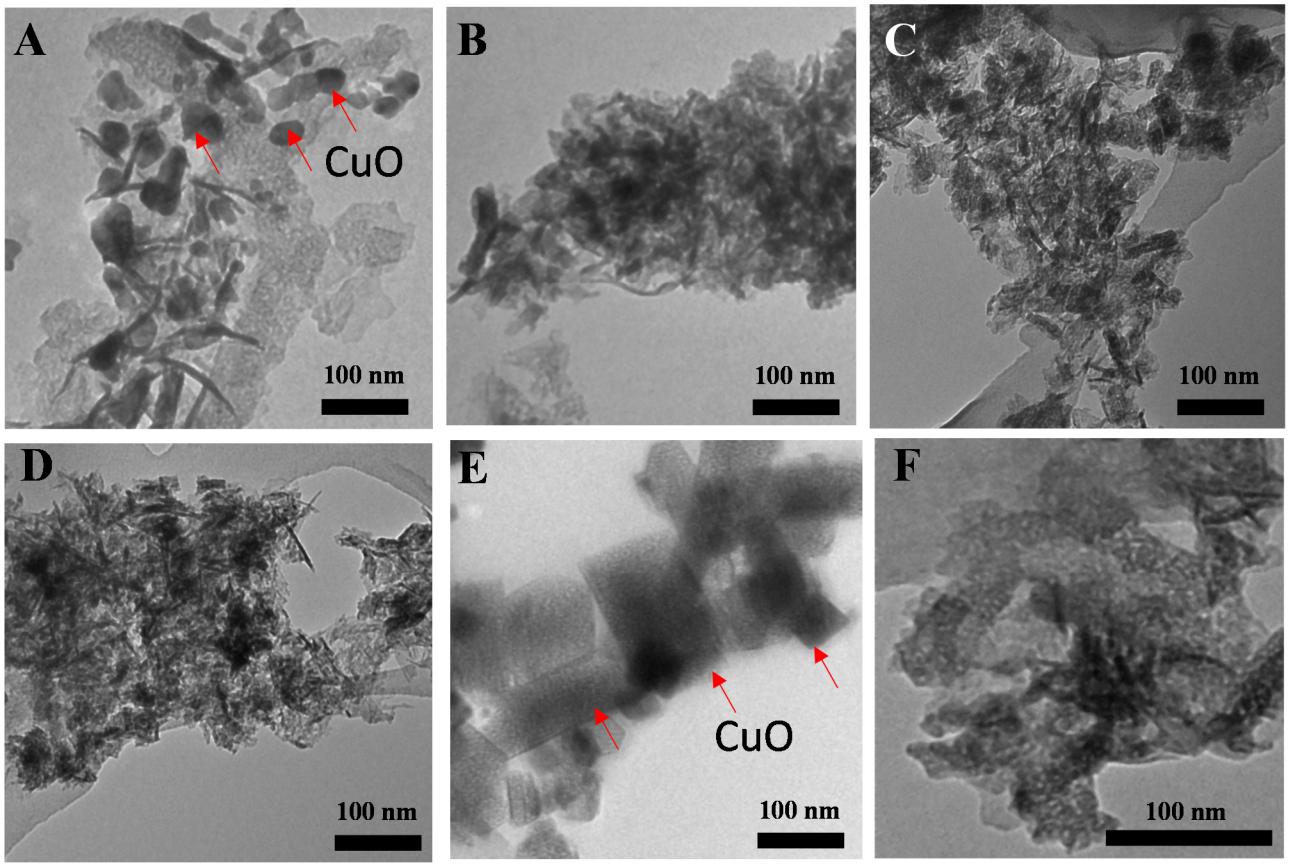


**Figure 2.** TEM images of the Cu-Ni/$Al_2O_4$ samples synthesized under different pH conditions: (**A**) 6.0, (**B**) 7.0, (**C**) 8.0, (**D**) 9.0, (**E**) 10.0, and (**F**) higher magnification image of pH 8 sample. (Note that calcination temperature is 600 °C for all samples).

### *2.2. Optimization of Hydrothermal Treatment Period and Formation Mechanism of Cu-Ni/$Al_2o_4$ Composite*

In the synthesis route proposed in the present study, hydrothermal processing is performed to improve the structural stability and dispersion of active sites in the synthesized mesoporous Cu-Ni/$Al_2O_4$ products through a dissolution and reconstruction process. Figure 3 shows the XRD patterns of the Cu-Ni/$Al_2O_4$ materials synthesized for different hydrothermal treatment times of 0 to 72 h followed by calcination at 600 °C. Without hydrothermal treatment, the XRD pattern of the calcined Cu-Ni/$Al_2O_4$ material contains two distinct peaks corresponding to CuO at 2θ = 35° and 38°, respectively. However, for the hydrothermally treated samples, all the XRD patterns show the existence of the $CuAl_2O_4$ amorphous phase with characteristic broad peaks at 2θ = 37° and 67°. In other words, these results confirm that hydrothermal reaction provides enough energy for the structural reconstruction between the metal hydroxides and the $Al(OH)_3$ support. In particular, the $Cu^{2+}$ and $Ni^{2+}$ ions can introduce into the $Al(OH)_3$ structure and form the mesoporous Cu-Ni/$Al_2O_4$ composition, as shown in reaction formula (1). In addition, part of the aluminum hydroxide is dehydrated during the hydrothermal treatment and forms AlOOH (see reaction formula (2). Finally, after calcination, the aluminum hydroxide and AlOOH are dehydrated to form γ-$Al_2O_3$ (see reaction formula 3) [30].

$$Cu(OH)_2 + 2Al(OH)_3 \rightleftharpoons CuAl_2O_4 + 4H_2O \quad (1)$$

$$Al(OH)_3 \rightleftharpoons AlOOH + H_2O \quad (2)$$

$$Al(OH)_3 + AlOOH \rightarrow Al_2O_3 + 2H_2O \quad (3)$$

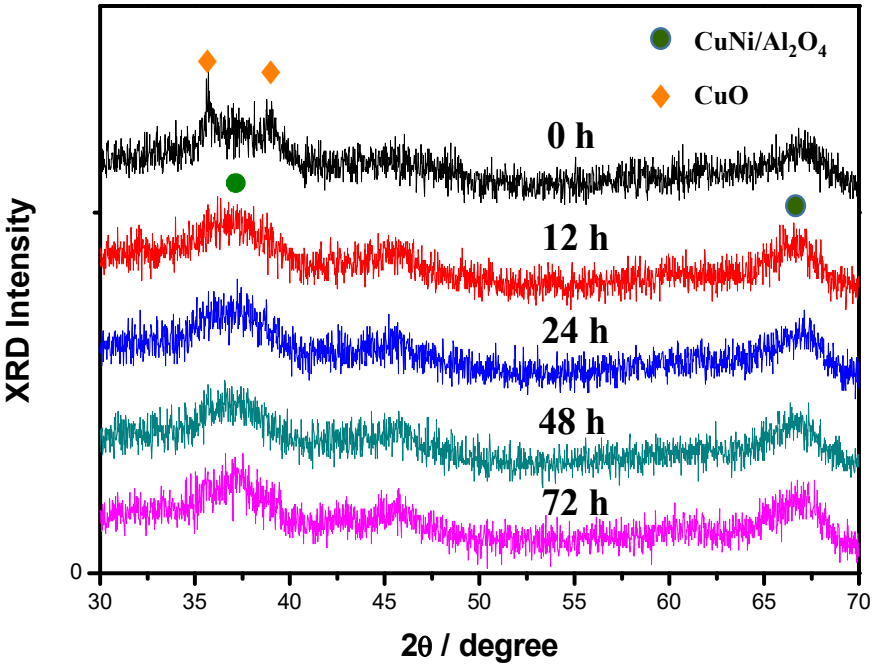


**Figure 3.** XRD patterns of the Cu-Ni/$Al_2O_4$ samples hydrothermally treated for different times. (Note that all samples were obtained from a calcination at 600 °C).

Figure 4 presents TEM images of the products synthesized using hydrothermal treatment times of 0 to 48 h and then calcined at 600 °C. The product calcined without hydrothermal processing has a long (400–500 nm) rod-like morphology (Figure 4A). However, following hydrothermal processing for 12 h, the rod-like structure is replaced with a short, sheet-like morphology (see Figure 4B). After a longer processing time of 24 h, the morphology transforms to a pure sheet-like structure with no obvious particle aggregation (Figure 4C). No significant change in the structure is observed at a longer hydrothermal processing time of 48 h (Figure 4D). Thus, for experimental convenience, and a lower cost, the optimal hydrothermal reaction time was chosen as 24 h for the following experiments.

Figure 5A shows the XRD patterns of the alumina and copper hydroxide/nickel hydroxide/alumina mixture, respectively, after hydrothermal reaction. For the alumina material, the XRD pattern shows distinct diffraction peaks corresponding to $Al(OH)_3$ and AlO(OH). Hence, it is inferred that the alumina has a high-crystalline structure following hydrothermal treatment. By contrast, the XRD pattern of the copper hydroxide/nickel hydroxide/alumina mixture shows weaker diffraction peak intensities of $Al(OH)_3$ and AlO(OH). Moreover, the related peaks are also significantly broader. In other words, the addition of $Cu^{2+}$ and $Ni^{2+}$ ions to the alumina mixture prompts a structural reorganization of $Al(OH)_3$ and suppresses the formation of high-crystallinity aluminum oxide, copper oxide and nickel oxide phases in the hydrothermal process. The TEM image in Figure 5B shows that, in the absence of metal ion addition, the calcination process prompts the formation of γ-alumina with a bulk stacked structure in a micrometer scale. By contrast, for the product with $Cu^{2+}$ and $Ni^{2+}$ ion addition, the calcination process transforms the alumina and the copper and nickel hydroxides into a porous Cu-Ni/$Al_2O_4$ structure with a sheet-like morphology, as shown in Figure 4C.

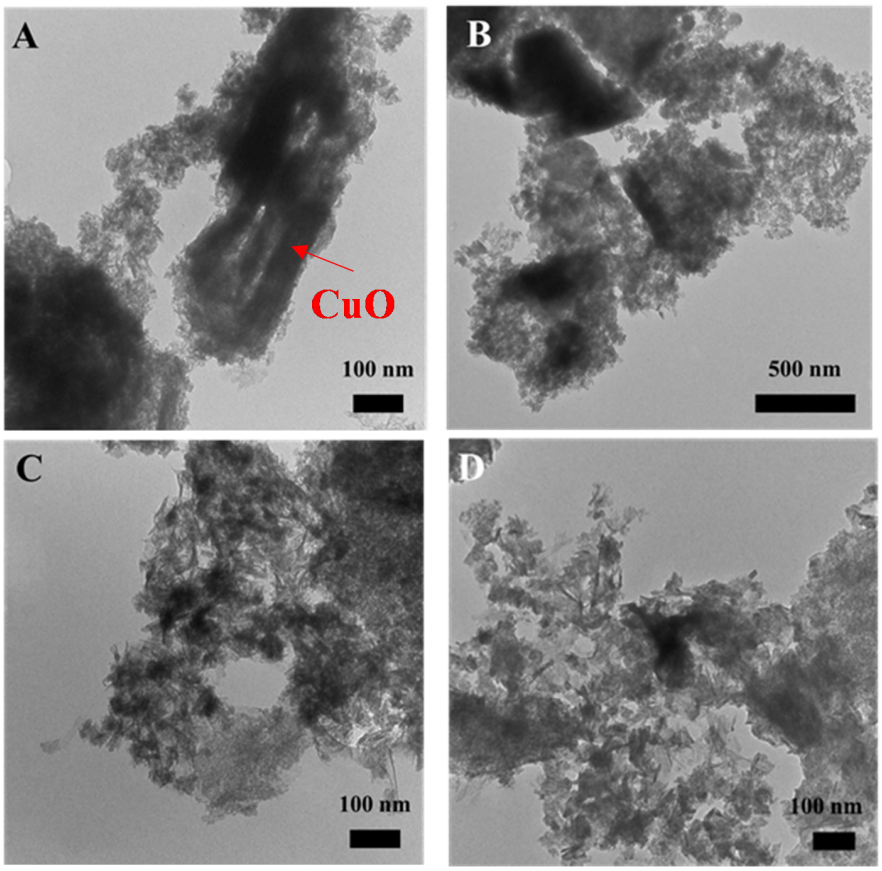


**Figure 4.** TEM images of the Cu-Ni/$Al_2O_4$ samples synthesized for different hydrothermal times: (**A**) 0 h, (**B**) 12 h, (**C**) 24 h, and (**D**) 48 h. (Note that all samples were obtained from a calcination at 600 °C).

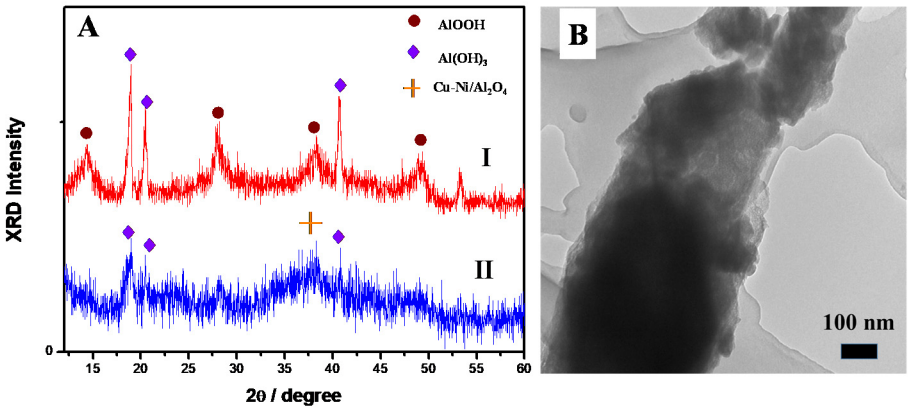


**Figure 5.** (**A**) XRD patterns of (I) active alumina and (II) copper hydroxide/nickel hydroxide/alumina mixture after hydrothermal reaction for 24 h. (**B**) TEM images ofalumina after calcination at 600 °C.

The results presented above suggest that the formation mechanism of the present Cu-Ni/$Al_2O_4$ materials. In particular, the activated alumina support dissolves into $Al(OH)_3$ and recrystallizes during the hydrothermal reaction process, and the $Cu^{2+}$, $Ni^{2+}$ and $Al(OH)_3$ then react to form a sheet-like structure under an appropriate pH environment of 7 to 9. At higher pH values (e.g., pH 10), the self-aggregation reaction of the $Cu^{2+}$ and $Ni^{2+}$ ions is too fast to combine with the $Al(OH)_3$. Consequently, the final product with a rod-like morphology contains a mixture of the high-crystallinity CuO, NiO and alumina.

### 2.3. Effect of Calcination Temperature on Cu-Ni/$Al_2O_4$ Composite and Its POM Application

The Cu-Ni/$Al_2O_4$ composites synthesized with a Ni:Cu:Al molar ratio of 1:10:100 at pH value of 9.0, a hydrothermal treatment temperature of 70 °C, and a hydrothermal treatment time of 24 h were found to have a high specific surface area (176 $m^2g^{-1}$) and good metal dispersibility. However, for catalysis applications, thermal treatment is required to achieve the essential crystallinity and textile properties [31,32]. Accordingly, the synthesized composites were further calcined at temperatures in the range of 600 to 800 °C in order to identify the optimal calcination temperature for POM applications. The XRD patterns presented in Figure 6A show that as the calcination temperature increases from 600 to 800 °C, the XRD intensity of the characteristic Cu-Ni/$Al_2O_4$ peaks increases. In other words, the crystallinity increases with an increasing calcination temperature. In addition, no characteristic XRD peaks ascribed to the NiO or CuO are observed, which confirms that both metal precursors are well dispersed in the alumina support without aggregation. Figure 6B shows that these three samples calcined at different temperatures have absorption peaks in the wavelength range of 1200 to 1700 nm, which implies that the $Cu^{2+}$ ions have a tetrahedral coordination in the crystalline phase of the prepared Cu-Ni/$Al_2O_4$ [33,34]. The absorbance intensity increases with an increasing calcination temperature that is hence consistent with the XRD finding of a greater crystallinity at a higher calcination temperature. Referring to Figure 6C, the composites calcined at temperatures of 600, 700 and 800 °C are found to have specific surface areas of 176 $m^2g^{-1}$, 131 $m^2g^{-1}$ and 82 $m^2g^{-1}$, respectively. The corresponding pore size varies from ca. 5 nm (600 °C) to ca. 11 nm (800 °C), as shown in Figure 6D. Overall, the results presented in Figure 6 confirm that the surface area and pore size of the Cu-Ni/$Al_2O_4$ catalyst can be readily controlled by adjusting the calcination temperature. Moreover, the results indicate that a calcination temperature of 600 °C is preferred for the POM applications due to the higher specific surface area and suitable pore size.

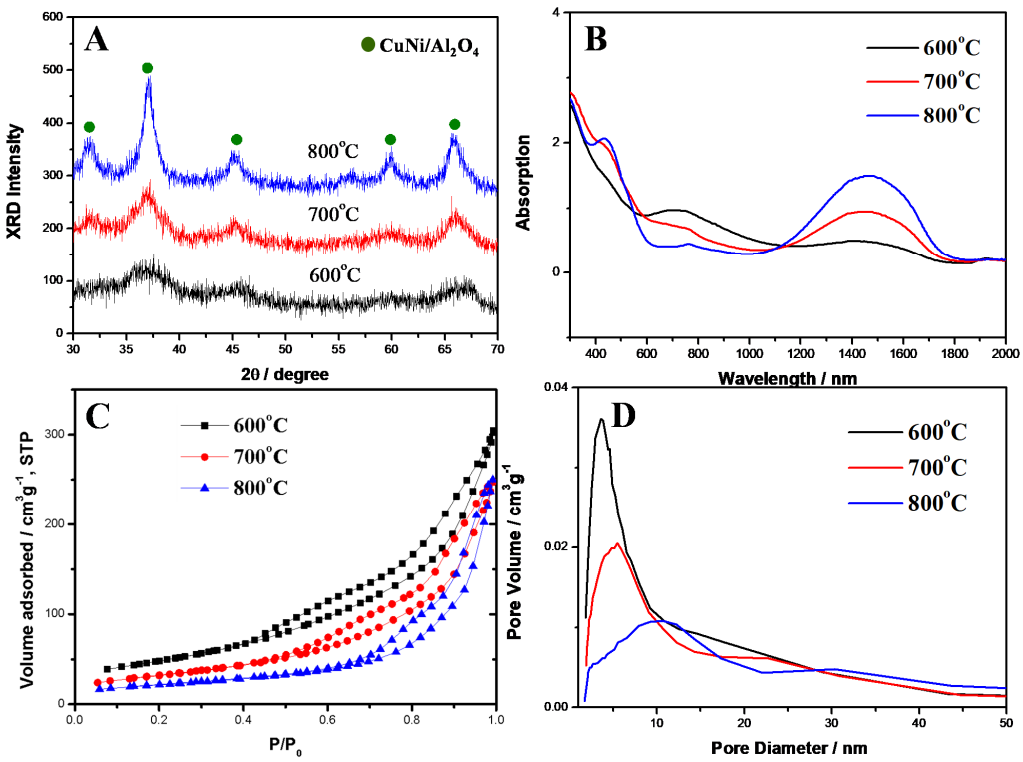


**Figure 6.** (**A**) XRD patterns, (**B**) DR-UV diagrams, (**C**) nitrogen adsorption and desorption isotherms, and (**D**) BJH pore size plots of the mesoporous Cu-Ni/$Al_2O_4$ samples synthesized at different calcination temperatures.

Figure 7 presents a schematic illustration of the POM reaction system used in the present study to produce hydrogen. For detailed experimental set up, please refer to Figure S1 (A schematic of the experimental system.) in supporting information. The POM reaction formula is as follows:

$$CH_3OH(aq) + \frac{1}{2}O_2(g) \rightleftharpoons 2H_2(g) + CO_2(g)\,\Delta H = -192.6\ (\mathrm{KJ\ mol^{-1}}) \quad (4)$$

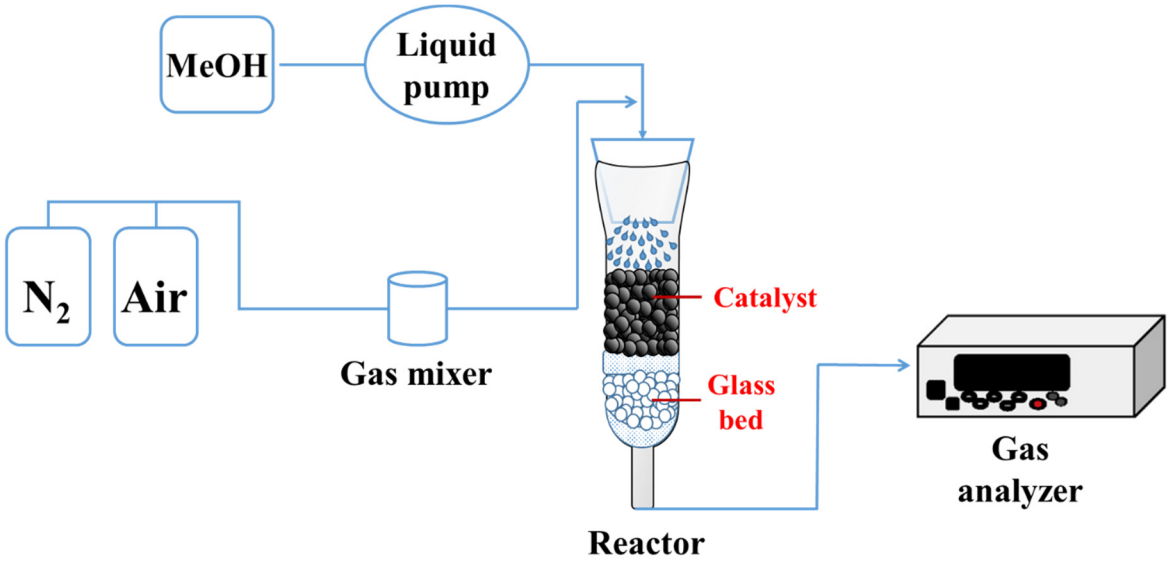


**Figure 7.** Schematic illustration of POM arrangement.

Temporal distributions of reaction temperature, MeOH conversion, $H_2$, CO, $CO_2$, and $CH_4$ concentrations for POM was shown in Figure 8. Furthermore, Table 2 compares the POM data for the present Cu-Ni/$Al_2O_4$ catalyst to those of two commercial platinum catalysts (Pt 0.2 wt% supported on $Al_2O_3$ & on BN-$Al_2O_3$ (boron nitride modified alumina), Green Hydrotech Inc. Taoyuan, Taiwan). As shown, the Pt/$Al_2O_3$ catalyst has a conversion rate of 93.5%, a hydrogen yield of 1.22 mol $H_2$/mol MeOH, and a minimal reaction temperature of 526 °C. Moreover, the catalyst has a carbon dioxide selectivity of 6.20% and a carbon monoxide selectivity of 5.40%. For the Pt/BN-$Al_2O_3$ catalyst, the conversion rate is increased to 98.35%, the selectivity of carbon dioxide is increased to 6.6%, and the selectivity of carbon monoxide is reduced to 5.10%. However, the hydrogen yield is also reduced to 1.18 mol $H_2$/mol MeOH, while the required reaction temperature is increased to 540 °C. For the present Cu-Ni/$Al_2O_4$ catalyst, the partial oxidation reaction requires a temperature of just 315 °C to proceed under equilibrium conditions. Notably, the methanol conversion rate reaches >99%, while the hydrogen yield increases to 1.99 mol $H_2$/mol MeOH. In addition, the carbon dioxide/carbon monoxide ratio is higher than those of the two commercial catalysts. In addition to the production of CO and $CO_2$, all three catalysts produce $CH_4$ in accordance with the reaction.

$$CO(g) + 3H_2(g) \rightleftharpoons CH_4(g) + H_2O(g) \qquad \Delta H = -205.9\ (\mathrm{KJ\ mol}) \quad (5)$$

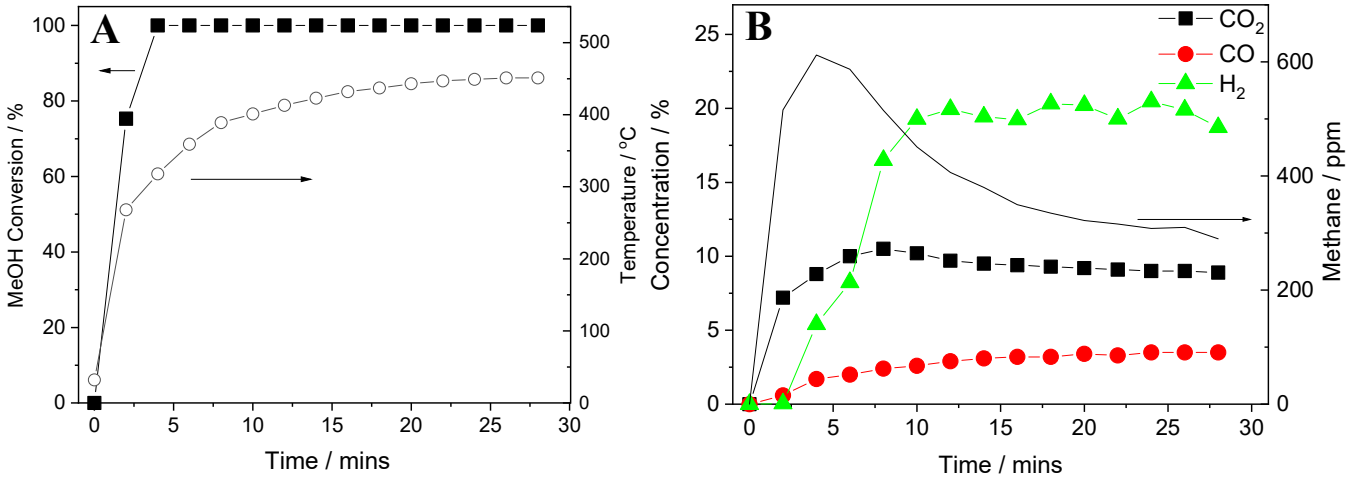


**Figure 8.** Temporal distributions of (**A**) MeOH conversion and temperature; (**B**) $H_2$, CO, $CO_2$, and $CH_4$ concentrations for POM.

**Table 2.** POM test data for different catalysts.

| Sample | GHSV ($h^{-1}$) | $O_2$/C | $CO_2$ (%) | CO (%) | $CH_4$ (ppm) | $H_2$ (%) | $CH_3OH$ Conversion (%) | $H_2$ Yield (mol/mol) | Temp (°C) |
|---|---|---|---|---|---|---|---|---|---|
| Pt/$Al_2O_3$ | 10,000 | 0.60 | 6.2 | 5.4 | 1887 | 14.48 | 93.5 | 1.22 | 526 |
| Pt/BN-$Al_2O_3$ | 10,000 | 0.60 | 6.6 | 5.1 | 1784 | 13.50 | 98.4 | 1.18 | 540 |
| Cu-Ni/$Al_2O_4$ | 10,000 | 0.60 | 9.1 | 3.3 | 290 | 20.46 | 100 | 1.99 | 315 |

The $CH_4$ production of the Cu-Ni/$Al_2O_4$ catalyst (290 ppm) is lower than that of either the Pt/$Al_2O_3$ catalyst (1887 ppm) or the Pt/BN-$Al_2O_3$ catalyst (1784 ppm).

The TEM images presented in Figure 9A,B show the morphologies of the Cu-Ni/$Al_2O_4$ composite before and after the catalytic reaction process, respectively. It is clearly seen that no obvious change occurs in the morphology during the reaction process that indicates the reacted Cu-Ni/$Al_2O_4$ composite retains a distinct mesoporous structure. The XRD patterns in Figure 9C show that the Cu-Ni/$Al_2O_4$ composites have characteristic peaks at $2\theta = 37°$ & $67°$ both before and after the reaction process, but the reacted sample has narrower peaks. The nitrogen adsorption and desorption curves presented in Figure 9D show that the porosity of the Cu-Ni/$Al_2O_4$ catalyst do not undergo significant decrease during the reaction process. For example, the specific surface area reduces only from 176 $m^2g^{-1}$ to 135 $m^2g^{-1}$. Overall, the results presented in Figure 9 indicate that the Cu-Ni/$Al_2O_4$ catalyst has good stability during the POM reaction.

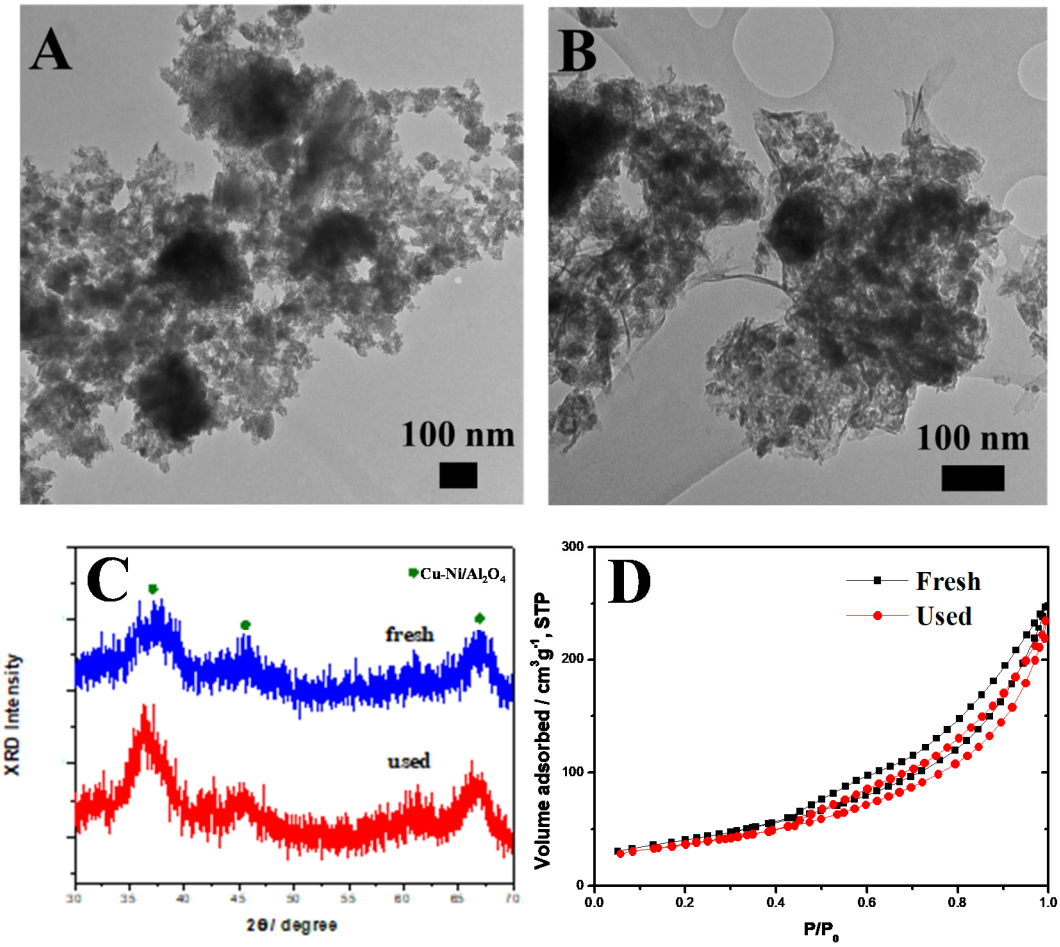


**Figure 9.** TEM images of Cu-Ni/$Al_2O_4$ catalyst (**A**) fresh catalyst and (**B**) after POM test. (**C**) XRD plots and (**D**) nitrogen adsorption-desorption isotherms of materials shown in (**A**,**B**).

## 3. Materials and Methods

### *3.1. Preparation of the Cu-Ni/$Al_2O_4$ Composite*

Typically, 1.5 g of copper (II) nitrate pentahemihydrate ($Cu(NO_3)_2$ $2.5H_2O$, >98%, J. T. Baker) and 0.196 g of nickel (II) nitrate hexahydrate ($Ni(NO_3)_2$ $6H_2O$, >98.5%, Merck) were dissolved in 100.0 mL of DI water. 2.53 g of activated alumina ($Al_2O_3$, Sigma-Aldrich) was separately dispersed in 80.0 mL of DI water. The copper and nickel ion solution was then added to the alumina solution. The pH value of the mixed gel solution was adjusted in the range of 6.0 to 10.0 through the addition of appropriate quantities of 2.0 M $NaOH_{(aq)}$ (sodium hydroxide 50 wt% in aqueous solution, AR®, Macron Fine Chemicals™). After stirring for 2.0 h at 40 °C, the gel solution was hydrothermally treated at 70 °C for different periods of 0, 3, 12, 24 and 72 h, respectively. Finally, the desired catalyst was obtained by filtration, drying and calcination at temperatures in the range of 600 to 800 °C.

### *3.2. Characterizations*

The $Cu^{2+}$ and $Ni^{2+}$ ion contents in the various products were measured by atomic absorption spectroscopy on an iCE 3300 Atomic Absorption Spectrometer (Thermo Fisher Scientific Inc., Taipei, Taiwan). The XRD patterns were taken with an X-ray diffractometer (Rigaku MultiFlex) (40 kV, 20 mA) using Cu $K_\alpha$ radiation. The $N_2$ sorption measurements were acquired using a surface area analyzer (Micromeritics TriStar II). In addition, the transmission electron microscope (TEM) observations were performed using a Hitachi H7500 microscope (80 kV). Finally, the interactions of the metal ions with the alumina matrix in the various samples were measured using a diffuse reflectance ultraviolet visible

spectroscope (DR-UV-vis, Hitachi U-4100). The gas analysis unit included a GA (gas analyzer, Fuji ZRJF5Y23-AERYR-YKLYYCY-A) and a GC (gas chromatography, SRI 310C TCD) to measure the volumetric concentrations of CO, $CO_2$, $CH_4$, and $H_2$.

### 3.3. Catalytic Tests

The POM reaction experiments were performed using a methanol flow rate of 1 mL $min^{-1}$, an $O_2$/C feed ratio of 0.6, and a gas hourly space velocity (GHSV) of 10,000 $h^{-1}$. Based on the flow rate and concentrations of CO, $CO_2$, and $CH_4$, methanol conversion rate can be calculated by the following Equation (6):

$$CH_3OH\ conversion\ (\%) = \left( \frac{\dot{n}_{CO_2,out} + \dot{n}_{CO,out} + \dot{n}_{CH_4,out}}{\dot{n}_{CH_3OH,in}} \right) \times 100 \quad (6)$$

where $\dot{n}$ stands for the molar flow rate (mol $min^{-1}$) and the subscripts "in" and "out" designate inflow and outflow, respectively. The $H_2$ yield can be estimated from the molar flow rate of hydrogen (mol $min^{-1}$) and $\dot{n}_{H_2}$ by the following Equation (7):

$$H_2\ yield\ (mol/mol\ CH_3OH) = \left( \frac{\dot{n}_{H_2}}{\dot{n}_{CH_3OH}} \right) \quad (7)$$

## 4. Conclusions

This study has presented a simple and green process for the preparation of the mesoporous Cu-Ni/$Al_2O_4$ composite material with a large surface area (>150 $m^2g^{-1}$). It has been shown that the mesoporous Cu-Ni/$Al_2O_4$ with a sheet-like morphology can be obtained at pH values in the range of 8.0~9.0 through hydrothermal treatment at 70 °C for 24 h followed by calcination at 600 °C. In line with the concept of green chemistry, the residual $Cu^{2+}$ and $Ni^{2+}$ ion concentrations in the filtrate solution following hydrothermal treatment are less than 1.0 ppm, and are hence consistent with the Taiwan effluent standard. Without the production of wastewater, this green synthetic method is suitable for the preparation of mesoporous Cu-Ni/$Al_2O_4$ catalysts. Finally, in the POM production of hydrogen, the Cu-Ni/$Al_2O_4$ catalyst achieves a high conversion efficiency (>99%) at a low reaction temperature of 315 °C. Overall, the synthesis method proposed herein provides a facile, green and scalable route for the production not only of Cu-Ni/$Al_2O_4$ catalysts, but also other mesoporous metal-alumina catalysts.

**Supplementary Materials:** The following are available online at https://www.mdpi.com/article/10.3390/catal12010032/s1, Figure S1: A schematic of the experimental system.

**Author Contributions:** Methodology, H.-P.L. and W.-H.C.; investigation, K.-J.L., Y.-K.C. and H.-K.H.; data curation, K.-J.L., Y.-K.C. and H.-K.H.; writing—review and editing, C.-H.H. and H.-P.L.; supervision, H.-P.L. and W.-H.C.; project administration, H.-P.L. and W.-H.C. All authors have read and agreed to the published version of the manuscript.

**Funding:** This work was supported by Ministry of Science and Technology, Taiwan, for the generous financial support of this research under Contract Nos. (MOST 110-2113-M-006-017 and MOST 110-2622-E-006-001-CC1).

**Institutional Review Board Statement:** Not applicable.

**Informed Consent Statement:** Not applicable.

**Data Availability Statement:** Not applicable.

**Acknowledgments:** The authors gratefully acknowledge the use of EM000800 & ICP000400 of MOST 110-2622-E-006-001-CC1 belonging to the Core Facility Center of National Cheng Kung University.

**Conflicts of Interest:** The authors declare no conflict of interest.

## References


1. Marinho, A.L.; Toniolo, F.S.; Noronha, F.B.; Epron, F.; Duprez, D.; Bion, N. Highly active and stable Ni dispersed on mesoporous $CeO_2$-$Al_2O_3$ catalysts for production of syngas by dry reforming of methane. *Appl. Catal. B Environ.* **2020**, *281*, 119459. [CrossRef]
2. Shafaghat, H.; Jae, J.; Jung, S.-C.; Jeon, J.-K.; Ko, C.H.; Park, Y.-K. Effect of methane co-feeding on product selectivity of catalytic pyrolysis of biomass. *Catal. Today* **2018**, *303*, 200–206. [CrossRef]
3. Iulianelli, A.; Ribeirinha, P.; Mendes, A.; Basile, A. Methanol steam reforming for hydrogen generation via conventional and membrane reactors: A review. *Renew. Sustain. Energy Rev.* **2014**, *29*, 355–368. [CrossRef]
4. Venvik, H.J.; Yang, J. Catalysis in microstructured reactors: Short review on small-scale syngas production and further conversion into methanol, DME and Fischer-Tropsch products. *Catal. Today* **2017**, *285*, 135–146. [CrossRef]
5. Sengodan, S.; Lan, R.; Humphreys, J.; Du, D.; Xu, W.; Wang, H.; Tao, S. Advances in reforming and partial oxidation of hydrocarbons for hydrogen production and fuel cell applications. *Renew. Sustain. Energy Rev.* **2018**, *82*, 761–780. [CrossRef]
6. Da Silva Veras, T.; Mozer, T.S.; da Costa Rubim Messeder dos Santos, D.; da Silva César, A. Hydrogen: Trends, production and characterization of the main process worldwide. *Int. J. Hydrog. Energy* **2017**, *42*, 2018–2033. [CrossRef]
7. Ghani, A.A.; Torabi, F.; Ibrahim, H. Autothermal reforming process for efficient hydrogen production from crude glycerol using nickel supported catalyst: Parametric and statistical analyses. *Energy* **2018**, *144*, 129–145. [CrossRef]
8. Sun, Z.; Zhang, X.; Li, H.; Liu, T.; Sang, S.; Chen, S.; Duan, L.; Zeng, L.; Xiang, W.; Gong, J. Chemical looping oxidative steam reforming of methanol: A new pathway for auto-thermal conversion. *Appl. Catal. B Environ.* **2020**, *269*, 118758. [CrossRef]
9. Chih, Y.-K.; Chen, W.-H.; Tran, K.-Q. Hydrogen production from methanol partial oxidation through the catalyst prepared using torrefaction liquid products. *Fuel* **2020**, *279*, 118419. [CrossRef]
10. Rednyk, A.; Ostroverkh, A.; Johánek, V. Hydrogen production via methanol oxidation on platinum oxide thin film catalyst: Influence of methanol-to-oxygen ratio. *Int. J. Hydrog. Energy* **2017**, *42*, 29254–29261. [CrossRef]
11. Li, S.; Ahmed, R.; Yi, Y.; Bogaerts, A. Methane to Methanol through Heterogeneous Catalysis and Plasma Catalysis. *Catalysts* **2021**, *11*, 590. [CrossRef]
12. Goula, M.; Kontou, S.K.; Tsiakaras, P.E. Hydrogen production by ethanol steam reforming over a commercial Pd/$\gamma$-$Al_2O_3$ catalyst. *Appl. Catal. B Environ.* **2004**, *49*, 135–144. [CrossRef]
13. Jiaguo, Y.; Lifang, Q.; Mietek, J. Hydrogen Production by Photocatalytic Water Splitting over Pt/$TiO_2$ Nanosheets with Exposed (001) Facets. *J. Phys. Chem. C* **2010**, *114*, 13118–13125.
14. Ju, C.; Li, M.; Fang, Y.; Tan, T. Efficient hydro-deoxygenation of lignin derived phenolic compounds over bifunctional catalysts with optimized acid/metal interactions. *Green Chem.* **2018**, *20*, 4492–4499. [CrossRef]
15. Auprêtre, F.; Descorme, C.; Duprez, D. Bio-ethanol catalytic steam reforming over supported metal catalysts. *Catal. Commun.* **2002**, *3*, 263–267. [CrossRef]
16. Tu, Y.-J.; Chen, Y.-W. Effects of Alkaline-Earth Oxide Additives on Silica-Supported Copper Catalysts in Ethanol Dehydrogenation. *Ind. Eng. Chem. Res.* **1998**, *37*, 2618–2622. [CrossRef]
17. Mariño, F.; Baronetti, G.; Jobbagy, M.; Laborde, M. Cu-Ni-K/$\gamma$-$Al_2O_3$ supported catalysts for ethanol steam reforming: Formation of hydrotalcite-type compounds as a result of metal–support interaction. *Appl. Catal. A Gen.* **2003**, *238*, 41–54. [CrossRef]
18. Hu, N.; Yang, C.; He, L.; Guan, Q.; Miao, R. Ni–Cu/$Al_2O_3$ catalysts for the selective hydrogenation of acetylene: A study on catalytic performance and reaction mechanism. *New J. Chem.* **2019**, *43*, 18120–18125. [CrossRef]
19. Ma, K.; Cui, Z.; Zhang, Z.; Huang, J.; Sun, Z.; Tian, Y.; Ding, T.; Li, X. Alloy-Mediated Ultra-Low CO Selectivity for Steam Reforming over Cu−Ni Bimetallic Catalysts. *ChemCatChem* **2018**, *10*, 4010–4017. [CrossRef]
20. Mosinska, M.; Stępińska, N.; Maniukiewicz, W.; Rogowski, J.; Mierczynska-Vasilev, A.; Vasilev, K.; Szynkowska, M.I.; Mierczynski, P. Hydrogen Production on Cu-Ni Catalysts via the Oxy-Steam Reforming of Methanol. *Catalysts* **2020**, *10*, 273. [CrossRef]
21. Charisiou, N.; Siakavelas, G.; Tzounis, L.; Dou, B.; Sebastian, V.; Hinder, S.; Baker, M.; Polychronopoulou, K.; Goula, M. Ni/$Y_2O_3$–$ZrO_2$ catalyst for hydrogen production through the glycerol steam reforming reaction. *Int. J. Hydrog. Energy* **2019**, *45*, 10442–10460. [CrossRef]
22. Kotnala, S.; Singh, L.; Gahtori, J.; Tucker, C.; Kumar, A.; Van Steen, E.; Bordoloi, A. Steam Reforming of Glycerol for Syngas Production using Pt–Ni Nanoparticles Supported on Bimodal Porous $MgAl_2O_4$. *Energy Fuels* **2021**, *35*, 5217–5230. [CrossRef]
23. Ortiz, W.G.C.; Delgado, D.; Fajardo, C.A.G.; Agouram, S.; Sanchís, R.; Solsona, B.; Nieto, J.M.L. Partial oxidation of methane and methanol on FeOx-, MoOx- and FeMoOx -$SiO_2$ catalysts prepared by sol-gel method: A comparative study. *Mol. Catal.* **2020**, *491*, 110982. [CrossRef]
24. Carrero, A.; Calles, J.A.; García-Moreno, L.; Vizcaíno, A.J. Production of Renewable Hydrogen from Glycerol Steam Reforming over Bimetallic Ni-(Cu,Co,Cr) Catalysts Supported on SBA-15 Silica. *Catalysts* **2017**, *7*, 55. [CrossRef]
25. Chen, W.-H.; Guo, Y.-Z. Hydrogen production characteristics of methanol partial oxidation under sprays with ultra-low Pt and Pd contents in catalysts. *Fuel* **2018**, *222*, 599–609. [CrossRef]
26. Lugo, V.R.; Mondragon-Galicia, G.; Gutierrez-Martinez, A.; Gutierrez-Wing, C.; Gonzalez, O.R.; Lopez, P.; Salinas-Hernandez, P.; Tzompantzi, F.; Valderrama, M.I.R.; Perez-Hernandez, R. Pt-Ni/ZnO-rod catalysts for hydrogen production by steam reforming of methanol with oxygen. *RSC Adv.* **2020**, *10*, 41315–41323. [CrossRef]
27. Huang, H.K.; Chih, Y.K.; Chen, W.H.; Hsu, C.Y.; Lin, K.J.; Lin, H.P.; Hsu, C.H. Synthesis and Regeneration of Mesoporous Ni-Cu/$Al_2O_4$ Catalyst in Sub-kilogram-Scale for Methanol Steam Reforming Reaction. *Int. J. Hydro. Energy*, 2022, in press. [CrossRef]

28. Chih, Y.-K.; Su, Y.-Q.; Chen, W.-H.; Lin, B.-J.; Kuo, J.-K.; You, S.; Lin, H.-P. Optimization for hydrogen production from methanol partial oxidation over Ni–Cu/$Al_2O_3$ catalyst under sprays. *Int. J. Hydrog. Energy*, 2021, in press. [CrossRef]
29. Chao, P.-Y.; Hsu, C.-H.; Lin, H.-P. Template-free synthesis of mesoporous $Mn_3O_4$-$Al_2O_3$ catalyst for low temperature selective catalytic reduction of NO with $NH_3$. *J. Taiwan Inst. Chem. Eng.* **2018**, *96*, 627–633. [CrossRef]
30. Shen, Y.C.; Hsu, C.H.; Lin, H.P. Biodegradable gelatin as template for preparation of mesoporous alumina. *J. Chin. Chem. Soc.* **2018**, *65*, 424–429. [CrossRef]
31. Chen, Y.; Chang, Y.; Hung, W.; Lin, H.; Shih, H.; Xie, W.; Li, S.; Hsu, C. Green synthesis of porous Ni-silicate catalyst for hydrogen generation via ammonia decomposition. *Int. J. Energy Res.* **2020**, *44*, 9748–9756. [CrossRef]
32. Wang, Y.; Liang, D.; Wang, C.; Chen, M.; Tang, Z.; Hu, J.; Yang, Z.; Zhang, H.; Wang, J.; Liu, S. Influence of calcination temperature of Ni/Attapulgite on hydrogen production by steam reforming ethanol. *Renew. Energy* **2020**, *160*, 597–611. [CrossRef]
33. Xie, S.; Zhang, X.; Tu, Q.; Shi, B.; Cui, Y.; Chen, C. Influence of Preparation Conditions on the Performance of Ni-Based Catalysts for Glycerol Steam Reforming. *ACS Omega* **2018**, *3*, 13335–13342. [CrossRef] [PubMed]
34. Tangcharoen, T.; T-Thienprasert, J.; Kongmark, C. Effect of calcination temperature on structural and optical properties of $MAl_2O_4$ (M = Ni, Cu, Zn) aluminate spinel nanoparticles. *J. Adv. Ceram.* **2019**, *8*, 352–366. [CrossRef]